Earth and Planetary Science Letters 450 (2016) 208–220

Contents lists available at ScienceDirect

Earth and Planetary Science Letters

www.elsevier.com/locate/epsl

Preconditioning and triggering of offshore slope failures and turbidity currents revealed by most detailed monitoring yet at a fjord-head delta

M.A. Clare [a,*], J.E. Hughes Clarke [b], P.J. Talling [a], M.J.B. Cartigny [a], D.G. Pratomo [c]

[a] National Oceanography Centre Southampton, European Way, Southampton, Hampshire, SO14 3ZH, United Kingdom
[b] Center for Coastal and Ocean Mapping, University of New Hampshire, USA
[c] Ocean Mapping Group, University of New Brunswick, Canada

ARTICLE INFO

Article history:
Received 25 February 2016
Received in revised form 13 June 2016
Accepted 15 June 2016
Available online 5 July 2016
Editor: M. Frank

Keywords:
river delta
submarine landslides
turbidity current
geohazard
mass failure
sediment flow

ABSTRACT

Rivers and turbidity currents are the two most important sediment transport processes by volume on Earth. Various hypotheses have been proposed for triggering of turbidity currents offshore from river mouths, including direct plunging of river discharge, delta mouth bar flushing or slope failure caused by low tides and gas expansion, earthquakes and rapid sedimentation. During 2011, 106 turbidity currents were monitored at Squamish Delta, British Columbia. This enables statistical analysis of timing, frequency and triggers. The largest peaks in river discharge did not create hyperpycnal flows. Instead, delayed delta-lip failures occurred 8–11 h after flood peaks, due to cumulative delta top sedimentation and tidally-induced pore pressure changes. Elevated river discharge is thus a significant control on the timing and rate of turbidity currents but not directly due to plunging river water. Elevated river discharge and focusing of river discharge at low tides cause increased sediment transport across the delta-lip, which is the most significant of all controls on flow timing in this setting.

1. Introduction

Rivers and offshore turbidity currents are the two most volumetrically important sediment transport processes on Earth, and form its most extensive sedimentary deposits (Ingersoll et al., 2003). It is important to understand how these two types of sediment-and-water flows are linked. For instance, how do changes in discharge from a river affect the frequency and character of turbidity currents, and how exactly are turbidity currents triggered immediately offshore from river mouths? Understanding controls on turbidity current frequency is also societally important as turbidity currents damage important seafloor infrastructure including telecommunications cables or pipelines (Carter et al., 2014), whilst submarine slope failures can trigger tsunamis (e.g. Prior et al., 1982).

River deltas can be sub-divided according factors that include the degree of wave or tidal action (Bhattacharya and Giosan, 2003), magnitude and type of river (e.g. bedload or suspended load-dominated; sand or gravel), offshore gradient, development of mouth bars and inertial or frictional mouth jets, and whether the river enters seawater or freshwater (Wright, 1977; Orton and Reading, 1993). Here we study offshore slope failure and turbidity currents generated at a marine fjord-head delta, which is one of the most common type of delta system globally. Fjord-head deltas are often characterised by limited fetch and hence wave heights, relatively steep offshore gradients, and coarse grained (sand or gravel) rivers with significant bedload transport from surrounding mountainous catchments. As with many other fjord head systems (e.g. Syvitski and Shaw, 1995), the delta that we study here is also affected by significant tides.

Multiple triggers are proposed for turbidity currents and landslides offshore from river mouths, including fjord-head systems (Fig. 1; Forel, 1888; Mulder et al., 2003; Piper and Normark, 2009). Debate surrounds the relative importance of these different triggers in river-fed systems, and there is a compelling need to test these alternative hypotheses (Fig. 1; Table 2). These preconditioning and triggering factors can be grouped into those due to plunging (hyperpycnal) river discharges that continue along the seafloor as turbidity currents, settling of sediment from a lower concentration surface (homopycnal) plume that generated underflows along the bed, or submerged slope failures that disintegrate to form turbidity currents. If sediment-laden river-water is dense enough to plunge, it continues to form a hyperpycnal turbidity current (Forel, 1888; Mulder and Syvitski, 1995; Parsons et al., 2001;

* Corresponding author.
E-mail address: m.clare@noc.ac.uk (M.A. Clare).

http://dx.doi.org/10.1016/j.epsl.2016.06.021

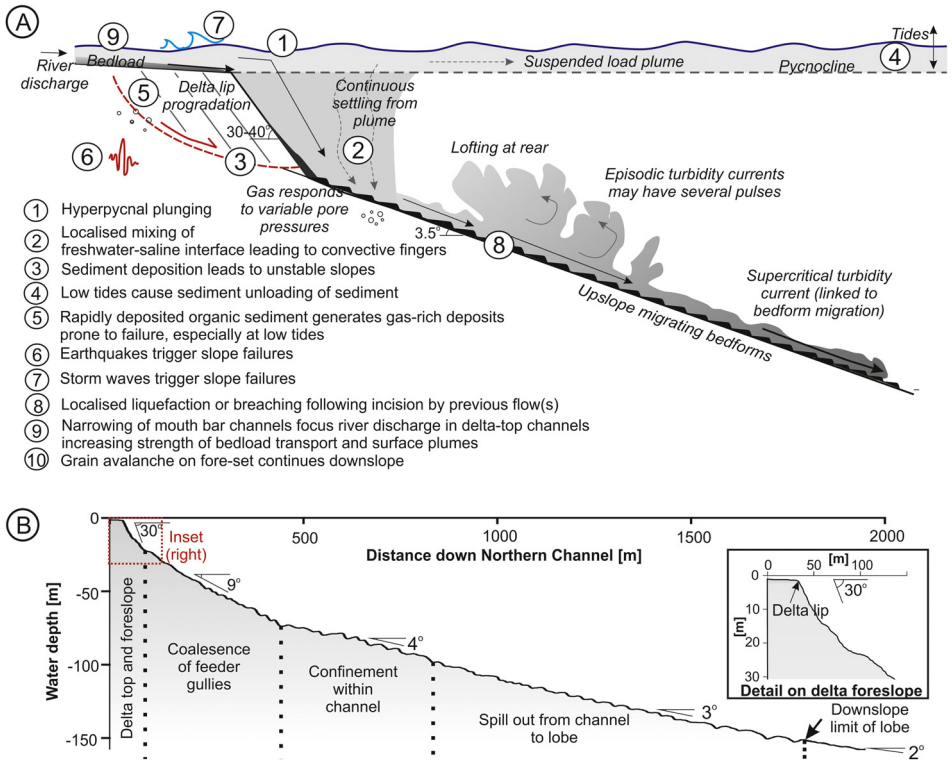

Fig. 1. (A) Previous hypotheses for triggering of slope failures and turbidity currents at fjord-head deltas with bedload-dominated rivers (upper panel; also see Table 2). (B) Water depth and slope angles based on Squamish delta slope (lower panel).

Mulder et al., 2003; label *1* in Fig. 1). Mixing of the freshwater-saline interface can cause enhanced settling of sediment due to convective fingers, at much lower (>1 kg/m^3) sediment concentrations (*2*; Parsons et al., 2001). As river flow expands at the coast, rapid sediment deposition can create unstable slopes prone to failure, resulting in turbidity currents (*3*, Prior et al., 1987; Carter et al., 2014). It has been proposed that slope failures can result from high excess pore pressures due to such rapid sedimentation, tidal unloading of sediments (*4*) and expansion of gas bubbles within organic rich deltaic sediment (*5*; Christian et al., 1997), earthquake shaking (*6*; Carter et al., 2014), or cyclic loading by storm waves (*7*; Prior et al., 1989). An initial turbidity current may cause failure by undercutting slopes, and contraction of sediment may create prolonged failures called breaches (*8*; Van Den Berg et al., 2002; Mastbergen and Van Den Berg, 2003). Low tides may also focus river discharge in delta-top channels thereby increasing significantly the strength of bedload transport and surface plumes (*9*; Prior et al., 1987; Hughes Clarke et al., 2012a; Dietrich et al., 2016). In areas of steep offshore topography, avalanching of sediment across the delta-lip may generate steep (30°) foresets that characterise Gilbert-type deltas (*10*; Gilbert, 1885; Postma et al., 1988).

However, these hypotheses are problematic to test as very few field data sets document the exact timing of turbidity currents and submerged slope failures, as they are difficult to monitor directly (Talling et al., 2015). Such information is key for determining the relative importance of river discharge, tides, or other triggering factors. No previous direct monitoring study has documented more than a few tens of turbidity currents; and in most cases far fewer (e.g. Prior et al., 1987 at Bute Inlet; Lambert and Giovanoli, 1988 in Lake Geneva; Cooper et al., 2013 in Congo Canyon; Carter et al., 2014 in Gaoping Canyon; Xu et al., 2014 in Monterey Canyon). Statistical analysis of event frequency and triggers has therefore been restricted to much less precisely dated ancient turbidity current and landslide events, with comparisons only possible with longer-term processes such as sea level change (e.g. Droxler and Schlager, 1985; Clare et al., 2014).

Here we present the first statistical analysis of >100 precisely-timed individual submarine landslide and turbidity current events from Squamish Delta in British Columbia, Canada (Hughes Clarke et al., 2012a, 2014). Event timing was determined from (i) a seafloor Acoustic Doppler Current Profiler (ADCP), and (ii) 93 approximately-daily repeat multibeam echo-sounder (MBES) surveys that document changes in seafloor morphology. This location represents arguably the most detailed monitoring of a turbidity current system that combines an exceptional number of repeat mapping surveys with direct flow measurements (Hughes Clarke et al., 2012a, 2012b, 2014; Hughes Clarke, 2016).

Three distinct types of event are recorded in this dataset (Hughes Clarke et al., 2012a, 2014). Infrequent, large-scale, deep-seated collapses of the prograding delta-lip are termed “delta-lip failures” More frequent events involve the upstream-migration of bedforms within channels on the submarine prodelta are termed “bedform events”. These bedform events may be further subdivided into those associated with an initial slope failure scar, and those that lack a visible (<0.5–1 m high) failure scar (“events without a headscar”).

2. Aims

Our overall aim is to understand the factors that precondition or trigger slope failure and turbidity currents on this fjord-head delta using an exceptionally detailed field data set. The first specific aim is to understand the factors that cause large-scale (>20,000 m^3) failures of the delta-lip, whilst the second aim is to understand the causes of bedform events. In the case of the second aim this includes statistical analysis of their relationship between the timing of these events and changes in river discharge and tidal elevation. Is river discharge or tidal elevation a stronger control, and do these two factors have independent or combined effects on

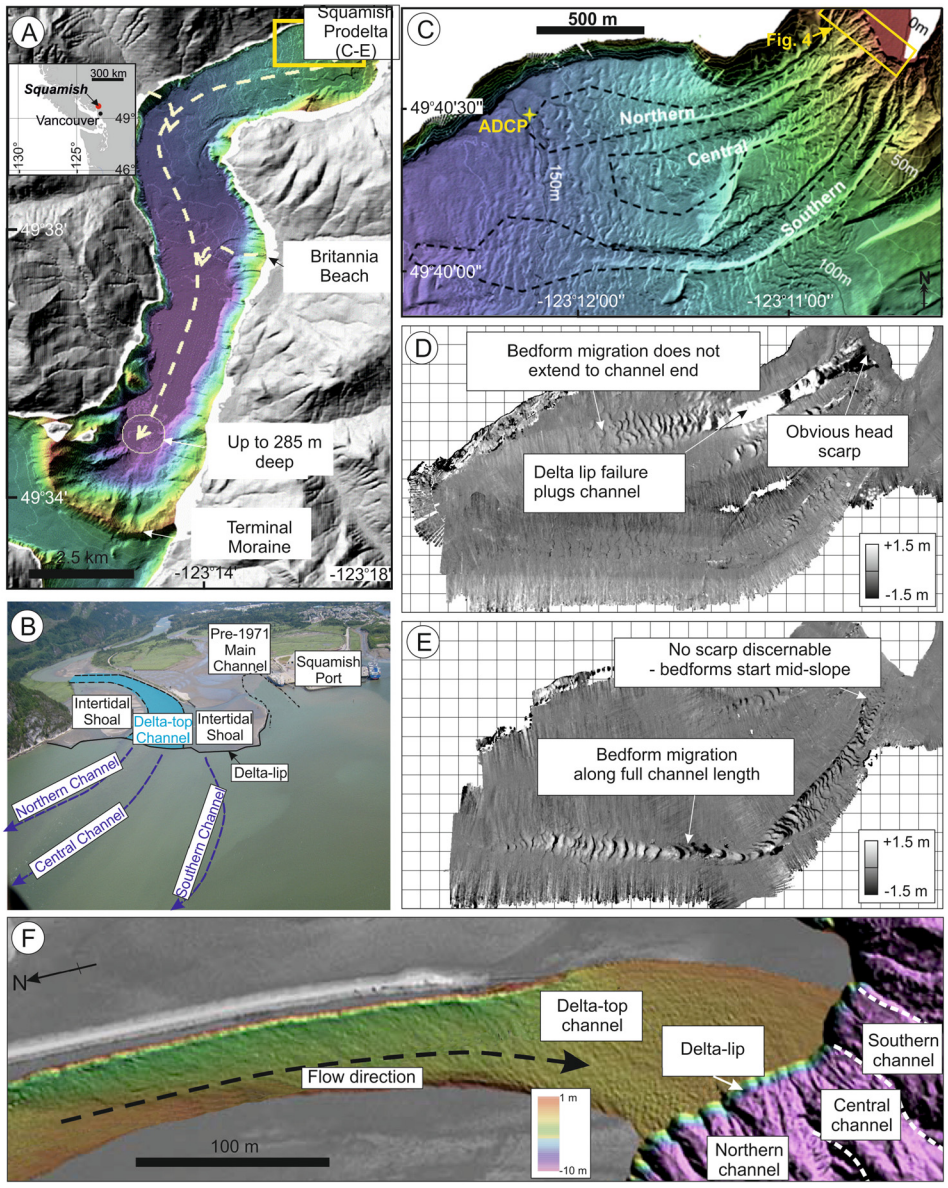

Fig. 2. (A) Squamish prodelta situated within the Upper Howe Sound, British Columbia showing extent of detailed bathymetry (yellow box) analysed in this paper. (B) Annotated aerial photograph showing location of delta-top channel. (C) Location of northern, central and southern channels at Squamish prodelta. ADCP location is yellow star at outflow of northern channel. Extent of Fig. 4 shown by yellow box; Difference maps of prodelta illustrating large delta lip failure in northern channel (D) and bedform event in southern channel without a headscar (E). (F) Perspective view of delta-top channel modified from Pratomo (2016). (For interpretation of the references to colour in this figure legend, the reader is referred to the web version of this article.)

turbidity current frequency? The implications of these associations are then discussed for understanding the physical mechanisms that trigger these flows.

3. Methods

3.1. Squamish delta: an outstanding natural laboratory

The Squamish River transports more than one million cubic metres of sediment per year to its delta and flows into Howe Sound (Fig. 2A; Hickin, 1989). The river is heavily influenced by seasonal meltwater, as the winter discharge of ~100 m^3/s increases in the freshet to >500 m^3/s, with peaks of up to 1000 m^3/s in summer. While enhanced suspended sediment occurs within the river plume during such discharge peaks, the values measured at more typical discharges (up to 0.4 kg/m^3) are much lower than that required to overcome the density surfeit (0.7 kg/m^3) for plunging river water (Hughes Clarke et al., 2014). Spring tidal range may reach 5 m whereas neap tides have a range of ~3 m. At low-water spring-tides, the river discharge is focused within a sub-tidal channel of 1 m depth and 200 m width where it reaches the delta-lip (Fig. 2B and F). This delta-top channel is flanked by two intertidal sand flats, and comprises dominantly sandy-gravel deposits with a mean grain size of ~0.5 to 0.8 mm. Seaward of the delta-lip, three main channels are found on the prodelta slope, termed "northern", "central" and "southern" channels. At a distance of 2 km from the delta-lip, these channels open out and flows become unconfined (Fig. 2C).

3.2. Bathymetric changes related to landslide and turbidity current activity

Squamish Delta is exceptionally well monitored as numerous multibeam surveys have been collected over eight years. 93 repeat surveys performed in 2011 enable the production of difference maps to observe daily change during the freshet. Changes in

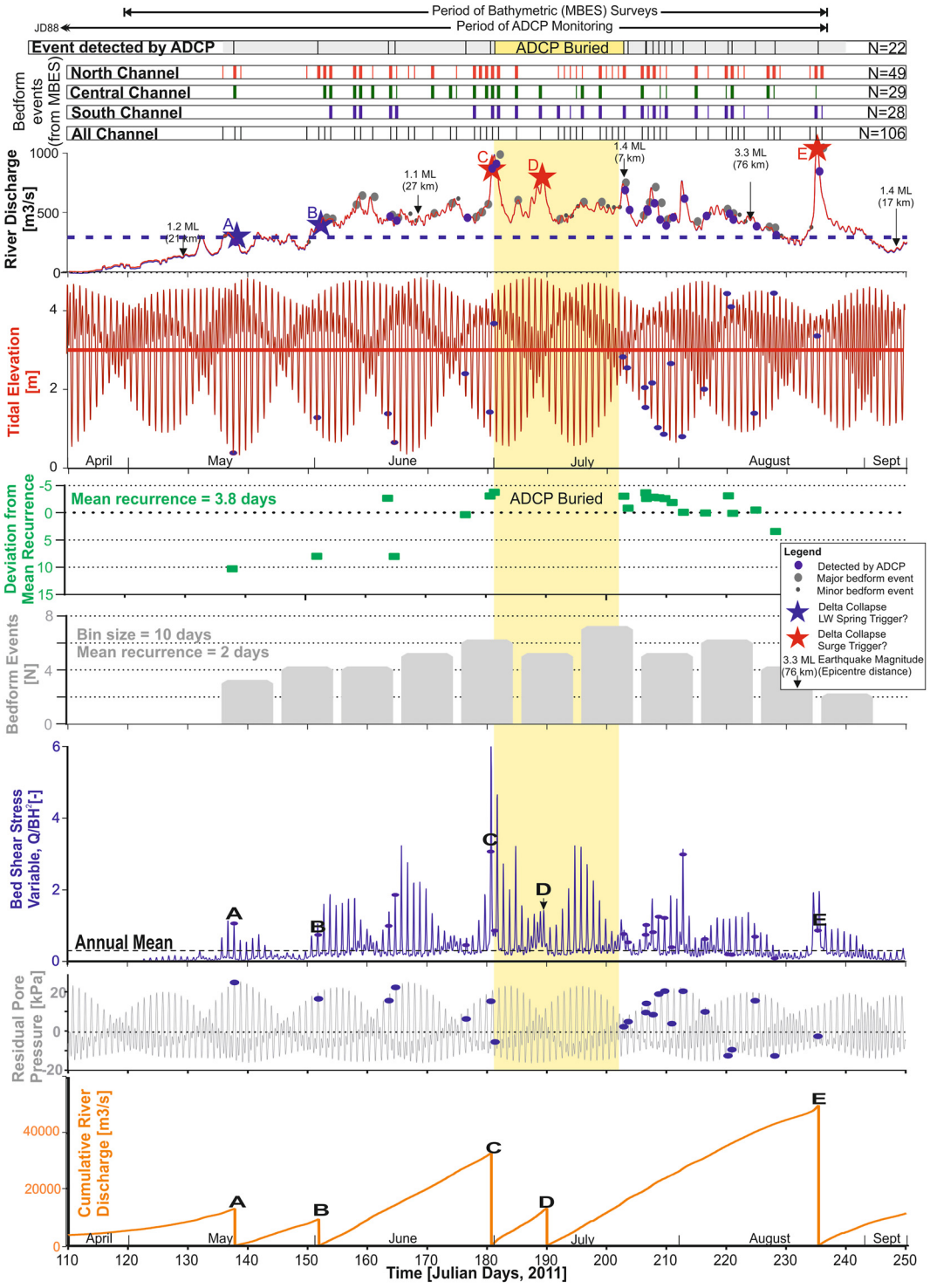

Fig. 3. Time series of event occurrence and variables discussed in this paper. Top four staves show timing of turbidity currents recorded by ADCP and bedform events detected from MBES (thicker bars denote major [>0.5 m] change; thinner bars denote minor [<0.5 m] change), river discharge and earthquakes, tidal elevation, recurrence of turbidity currents detected at ADCP location, bedform event frequency per 10 day bins, delta-top bed shear stress variable, residual pore pressure at 10 m below seafloor, and cumulative river discharge leading up to delta-lip collapses A to E (annotated).

seafloor morphology have been shown to be related to slope failures and turbidity currents (Hughes Clarke et al., 2012a, 2012b, 2014). Water column imaging above bedforms in the prodelta channels has clearly imaged active turbidity currents that locally erode and deposit sediment (Hughes Clarke, 2016).

The first observed type of bathymetric change relates to "delta-lip collapses" – large (>20,000 m^3) failures of the delta front. Five such events were observed in 2011; referred to here as delta-lip collapses A to E (Figs. 3 and 4).

The second type of bathymetric change relates to upstream migration of channel bedforms ('bedform events'). Based on analogies with laboratory experiments, supported by recent water column imaging, bedform migration is inferred to result from turbidity currents that generate cyclic steps (Hughes Clarke et al., 2012b, 2014;

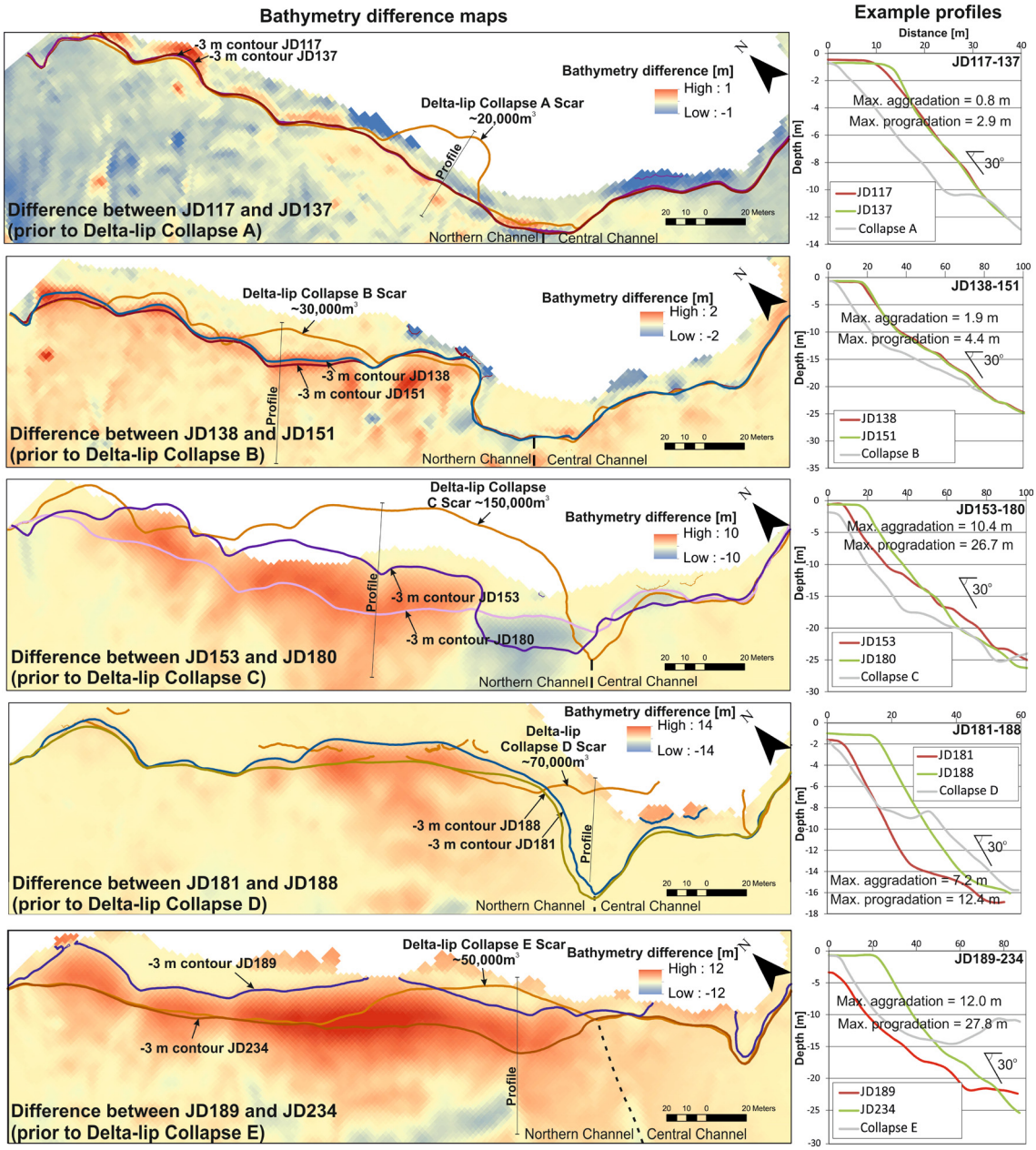

Fig. 4. Bathymetry difference maps (left panels) for time periods building up to a delta-lip collapse. River flow is from the top. Location of maps is shown in Fig. 2C. Changes in bathymetric depths are shown for time period between the day of a delta-lip failure and the day before the next delta-lip failure. Hot colours (red) illustrate higher net sediment accumulation. Cool colours (blue) illustrate net sediment loss. Colour scales differ on each panel. The approximate position of the delta-lip is shown by lines denoting the −3 m water depth contour at the start and end of each period. Also shown is the extent of the failure scar for each delta-lip collapse. The division between the Northern and Central Channels is depicted by dotted line, and only Delta-lip Failure D (JD189) did not occur at the head of the Northern Channel. Example bathymetric profiles (right panels) are presented for the start (red) and end (green) of each period, as well as the profile that resulted from each delta-lip failure event (grey). (For interpretation of the references to colour in this figure legend, the reader is referred to the web version of this article.)

Hughes Clarke, 2016; Symons et al., 2016). As event timing can only be constrained to the nearest ∼24 h, the minimum recurrence interval that can be resolved is one day for MBES observations. The precise temporal resolution may vary between ∼20 and 30 h, depending on when a particular feature (e.g. delta lip) was surveyed on successive days. A total of 106 discrete bedform events were identified from the MBES data, with 49 in the north, 29 in the central and 28 in the south channel (Fig. 3). We sub-divide these 'bedform events' based on the morphology at their upslope limit. Some bedform events include smaller-scale failures near the delta-lip ('bedform events with headscars'), but others start mid-slope (typically at ∼20 m water depth) without an obvious landslide scar ('bedform events without headscars'; Fig. 2D&E). We also classify the amount of vertical change related to each bedform event. Clearly noticeable change of >0.5 m is significantly above the resolution of MBES and is termed "major" change. "Minor" change is defined as <0.5 m vertical difference.

3.3. Direct monitoring of turbidity currents using an ADCP

An upward-looking 600 kHz ADCP was installed for 147 days downstream of the northern channel (Fig. 2C). This ADCP recorded the arrival of turbidity currents to within 30 s. Deployment was continuous from 29/03/11 to 23/08/11 (Julian Day 088-235), with the exception of a 20 day period from 30/6/11 to 20/07/11 (JD181-201) when the ADCP was buried by the run-out from a ma-

jor delta-lip failure event. MBES repeat surveys defined 49 bedform events relating to turbidity currents that caused morphological change in the northern channel. However, only 22 turbidity currents were recorded at the more distal ADCP location (Fig. 3). At the ADCP location, flow speeds were recorded in the region of 0.3 to 1.5 m/s, with thicknesses from 10 m to 40 m, with some lasting for over 1 h. Material suspended by turbidity currents took more than 8 h to settle out (Hughes Clarke et al., 2012b).

The variables considered as causes here include tides, river discharge and earthquakes. Hourly tidal measurements in metres relative to mean sea level were used (Hughes Clarke et al., 2012a, 2012a). Hourly river discharge data, recorded in m^3/s, from September 2010 to November 2011 were obtained 12 km upstream at Brackendale, Environmental Canada station 08GA022. The timing and magnitude of earthquake events are from the Earthquakes Canada database (http://earthquakescanada.nrcan.gc.ca/stndon/NEDB-BNDS/bull-eng.php). In some locations worldwide, turbidity currents coincide with larger wave heights (Xu et al., 2004). However, because the Squamish Delta has limited fetch it experiences small wave heights (Stronach et al., 2006), and consequently wave height is excluded from this analysis. Non-parametric statistical tests (Mann–Whitney and Kolmogorov Smirnov) are used to determine whether specific conditions (river discharge and tidal state) correlate with the *timing* of a turbidity current, or if they cannot be discerned from a scenario in which turbidity currents are randomly triggered. Generalised Linear and Proportional Hazard Models (Clare et al., 2016 and references therein; Appendix A) then test for the significance of the same variables on the *rate* at which turbidity currents occur.

4. Results

4.1. Delta-lip collapses

Slope instability typically arises under one or more conditions that can include i) over-steepening of the slope through differential deposition; ii) loading of the upper slope by sediment; iii) removal of sediment from the toe of the slope; and iv) changes in pore pressure regime (Bromhead, 2006). The latter can be caused by rapid sedimentation (where insufficient time exists to allow dissipation of excess pore pressures), the presence of gas in pore spaces otherwise filled with water, and transient perturbations such as cyclic storm wave loading, earthquake activity, and hydraulic fluctuations due to the tidal cycle. The rate of pore pressure dissipation is governed by the diffusion pathway distance (thickness of overburden) and the coefficient of consolidation (c_v), which is in turn a function of permeability and sediment compressibility (Terzaghi, 1943). Here we investigate how such processes may have preconditioned and triggered large collapses of the delta-lip.

Delta-lip collapses A, B, C and E occurred at the head of the Northern Channel, while D was at the head of the Central Channel (Fig. 4). On each of the days within which a delta-lip collapse was determined from MBES surveying at the head of the Northern Channel, we also detect a turbidity current at the ADCP location. We assume that these particular turbidity currents were directly related to run-out from the delta-lip collapse and not to an initial hyperpycnal flow. River concentrations were too low for hyperpycnal flow conditions (Hughes Clarke et al., 2014) and the presence of large scars on the delta lip (Fig. 4) support this assumption. We thus use the more precisely constrained ADCP monitoring to determine the timing of delta lip failures A, B, C and E. As delta-lip collapse D occurred at the head of the Central Channel, and during the period under which the ADCP had been buried, it is not possible to provide a more precise timing for that specific event.

The first two major delta-lip collapses we detected (A and B) coincided with relatively low spring tides (0.25 and 0.69 m respectively), but not peaks in river discharge (Figs. 3 and 6; Hughes Clarke et al., 2012a). Subsequent delta-lip collapses (C, D and E) occurred shortly (8–11 h) after the three largest river discharge peaks (>775 m^3/s). The largest delta-lip collapse (C), that buried the ADCP, occurred ~8 h (+/− ~ 15 min) after the second highest recorded river discharge. While there are differences in the instantaneous discharge for these events, the cumulative river discharge prior to failure is above a minimum threshold (>90,000 m^3/s) for all delta-lip collapses (Fig. 3). Difference maps show the accumulation of sediment at the delta-lip (Fig. 4). Sediment accumulation at the delta-lip, prior to each lip failure (presented as maximum vertical aggradation/seaward progradation) was: 0.8 m/2.9 m (A), 1.9 m/4.4 m (B), 10.4 m/26.7 m (C), 7.2 m/12.4 m (D), 12.0 m/27.8 m (E). Based on sediments sampled from the Fraser River delta slope, dissipation of excess pore pressures due to the additional sediment deposited prior to delta-lip collapses C, D and E would have taken weeks to months (Fig. 5). The mean grain size for the Fraser River prodelta slope is c. 0.25 mm (Chillarige et al., 1997) compared to 0.5–0.8 mm for the Squamish delta top, and 0.1–0.2 mm for the Squamish prodelta slope (as measured from grab samples), so that analogy is not entirely unreasonable. However, Fraser River sediments feature a higher proportion of fine sediments than Squamish which would promote longer pore pressure dissipation times. The presence of gas hosted in pores will also inhibit dissipation (Fig. 5). Squamish delta slope sediments host considerable amounts of gas (Hughes Clarke et al., 2012b), but precise quantities are not known at this time. Hence, some degree of uncertainty exists on the exact time for excess pore pressure dissipation. The smaller loads applied prior to delta-lip collapses A and B may have been less significant, but the tidal-induced pore pressure effects may have been more pronounced for these events in May and early June.

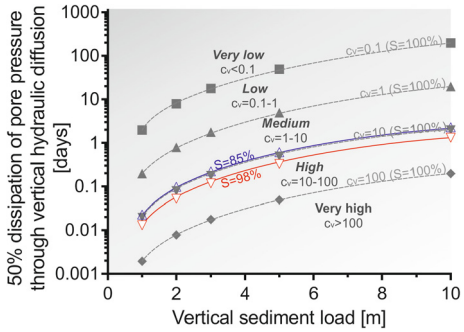

Fig. 5. Time required for 50% dissipation of excess pore pressures following instantaneous sediment loading of variable thickness. The time to dissipate pore pressures is highly dependent on the consolidation (or hydraulic diffusivity) coefficient (c_v, m^2/yr) and the degree of pore fluid saturation (S), where S = 98% equates to 2% gas saturation. Hollow symbols based on values from Fraser River for different gas saturations (S = 85% and 98%) (Chillarige et al., 1997). Filled symbols illustrate sensitivity of dissipation times for the full range of consolidation rates defined in Lambe and Whitman (2008). Results based on methods in Terzaghi (1943).

4.2. Triggering of events during river floods – via hyperpycnal flow or slope failure?

Previous work has suggested that plunging river floodwater may trigger turbidity currents (Forel, 1888; Mulder et al., 2003), but Hughes Clarke et al. (2014) has shown that the density threshold required for hyperpycnal flow is not achieved at Squamish for the discharges seen here. ADCP data shows that delta-lip collapses (C and E) occurred ~8 to 11 h after the peak in river discharge (Fig. 6). Delays cannot be determined for delta-lip collapse D as the ADCP was temporarily buried. The peak in river discharge should also equate to the peak in sediment transport from the river, as the suspended sediment concentration for Squamish River is higher

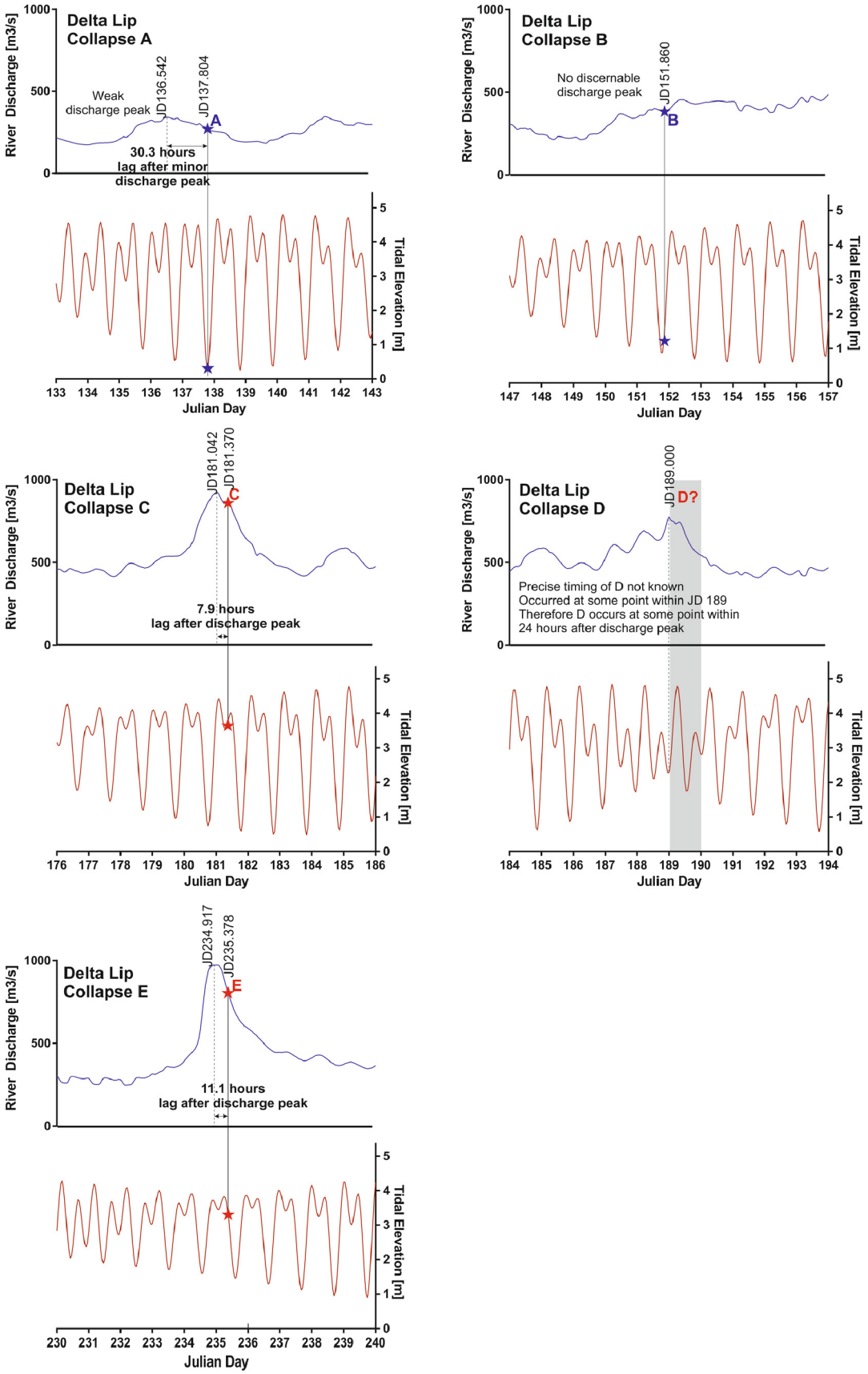

Fig. 6. Time series of river discharge and tidal elevation during delta lip failure events A to E. Timing of delta-lip failures is based on measurements from the ADCP at the end of the Northern Channel. As delta-lip failure D occurred at the top of the Central Channel, and during a time at which the ADCP was buried, the precise timing of delta lip collapse D could not be identified. A major event was noted from the MBES data during JD189; hence event D occurred at some point after a river discharge peak at JD189.0. Therefore it can be inferred there was some time lag, albeit unquantified. River discharge measured at a station 12 km upstream.

Table 1
Results of non-parametric statistical tests to determine significance of difference between annual range in variables against the range coincident with events detected by the ADCP. Bold italicised values are significantly different ($p < 0.05$).

Test type		River discharge	Tidal elevation	Residual pore pressure
Kolmogorov–Smirnov	*p*-value	***0.0005***	***<0.0001***	***0.0017***
	Kolmogorov–Smirnov D	0.4330	0.5492	0.4021
Mann–Whitney	*p*-value	***<0.0001***	***0.0002***	***0.0005***
	Mann–Whitney U	25918	30300	32070
	Difference: Actual	186.7	−1.320	12.12
	Difference: Hodges–Lehmann	221.1	−1.110	8.929
	95% Confidence Interval	140.1 to 301.3	−1.630 to −0.055	9.09 to 19.39

on the rising limb of a flood (Hickin, 1989). Based on conservative river velocities of 1 to 3 m/s measured near and downstream from the discharge monitoring station during a flood peak (Hickin, 1989), it is calculated that river discharge would reach the delta-lip within 1 to 3 h. This analysis also assumed that submarine flows took ~30 min to travel from the delta-lip to the ADCP mooring at a speed of 1 m/s which is consistent with that measured by the ADCP (Hughes Clarke et al., 2012b). The observed lag of 8 to 11 h post-discharge peak is therefore not explained by the potential maximum lag of 3.5 h for discharge to reach the ADCP. Delta-lip failure therefore post-dates the peak of flood discharge by several hours. Furthermore, headscarps seen in MBES data show clearly that the initiation mechanism for events C, D and E was slope failure, rather than plunging hyperpycnal river discharge (Fig. 4; Hughes Clarke et al., 2014).

4.3. Did earthquakes trigger delta-lip collapses or turbidity currents?

Only one earthquake of >2 M_L occurred during the monitoring period (76 km to the south-east, 3.3 M_L on JD 224.25), but it did not coincide with any turbidity current or delta-lip collapse events. Two <2 M_L earthquakes occurred within 30 km of Squamish in the same period, one of which preceded an event observed on the ADCP by ~8 h, and the other by ~8 days (Fig. 3). Therefore, small <3.3 M_L earthquakes did not trigger slope failures or turbidity currents, during the 2011 monitoring period. The influence of larger earthquakes or series of small earthquakes cannot be determined because neither occurred during the monitoring period.

4.4. Does river discharge control the 'switch on' and recurrence rate of turbidity currents?

We now discuss the triggering of bedform events that are not associated with large delta-lip failures. Only the first of the bedform events occurred when river discharge was below the annual average discharge (253 m^3/s). This first bedform event did, however, occur 24 h after a discharge peak of 342 m^3/s. More than three quarters of bedform events occurred when river discharge was >75% of its annual range (Fig. 7); which is a highly significant difference ($p < 0.0001$) for *event timing* (Table 1).

The general trend of increasing river discharge towards the freshet peak in June and July is mirrored by more frequent turbidity current activity (Fig. 3). The number of bedform events detected per 10 day bin was more than double (1 event every 1.43 days) than at the start (1 event every 3.33 days) of the freshet (Fig. 3). The frequency of turbidity currents directly detected by the ADCP also increased, particularly between JD180-225 (1 event/3.8 days). River discharge is also shown to be a strongly significant variable on event *recurrence rate*. Both Proportional Hazard ($p = 0.002$–0.0008) and Generalised Linear Models ($p = 0.002$–0.003) indicate that river discharge is highly significant in relation to flow recurrence rate.

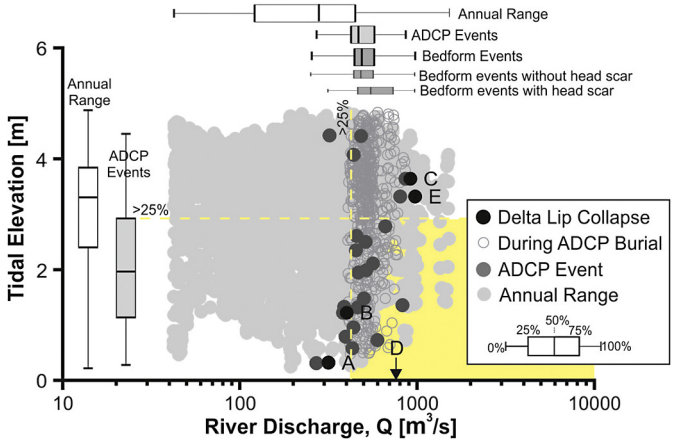

Fig. 7. Comparison of background annual variations in tidal elevation and river discharge with those at the time of observed turbidity currents detected by the ADCP. Box and whiskers demonstrate the range of conditions, where whiskers cover the full range of data and boxes show 25th, 50th and 75th percentiles. Dark grey solid circles are conditions at the time of turbidity currents detected by the ADCP. Black solid circles are conditions at delta-lip collapses. Light grey solid circles are conditions during which no events were observed. Hollow circles indicate the period during which the ADCP was buried, and hence it is not known if any events occurred or not. As the ADCP was buried during delta-lip collapse D, only the approximate river discharge can be quantified (arrow on *x* axis). Yellow fill indicates range of conditions within which 75% of events occurred. (For interpretation of the references to colour in this figure legend, the reader is referred to the web version of this article.)

4.5. Do delta-lip collapses and turbidity currents coincide with low tides?

Two major delta-lip collapses (A and B) correspond to relatively lower river discharge conditions compared with the rest of the freshet (<480 m^3/s). These events occurred during relatively low minimum spring tides; 2.8 m and 1.9 m below the mean annual tidal elevation for the A and B delta-lip collapses respectively (Fig. 3). While the three other delta-lip collapse events correspond to extreme river discharges, they also correspond to tidal elevations that are lower than 75% of the annual conditions (Fig. 7). The tidal elevation at the initiation time of turbidity currents unrelated to delta-lip collapses is also significantly different to that of the annual range (Fig. 3), and is unlikely to be due to random chance (Mann–Whitney test, $p = 0.0002$; Kolmogorov–Smirnov test, $p = 0.0005$; Table 1).

Tidal loading may cause shallow slope failure by liquefaction (Kramer, 1988). However, this process cannot explain the largest delta-lip collapses, due to the depth of their failure surface (>10 m). Changes in subsurface pore–water pressure due to tidal drawdown are probably more important – particularly in gas-saturated sediments. Squamish Prodelta sediments are known to be gas saturated (Hughes Clarke et al., 2012a). Pore–water pressure response is calculated at 10 m below seafloor based on the method

in Chillarige et al. (1997), which was developed for a similar site at the Fraser River Delta, British Columbia (full method is presented in Appendix A; Fig. 3). Similarly to the tidal analysis, pore pressures during the events are found to be significantly different to those for the annual range ($p = 0.0005$–0.0017), with most events occurring at times featuring positive residual pore pressures (i.e. coincident with lowered hydrostatic pressure).

4.6. Does turbidity current timing relate to a combination of tide and river discharge effects?

The next step is to relate river discharge and tidal elevation in a simple manner to bed shear stress, and hence the rate at which bedload drives sediment over the delta-lip. Bed shear stress controls rates of bedload transport by the river to the delta-lip, and hence rates of sediment deposition and lip migration (Pratomo, 2016). Here, a bed shear stress variable, Q/BH^2, is derived at the delta-lip, where Q is river discharge, and B and H are the delta-top channel width and height respectively (Appendix A). A rectangular channel is assumed, so that H changes in response to tidal fluctuations, but B remains constant. Thus, the output is conservative because if a U- or V-shaped channel was considered, the channel width, B, would be considerably narrower during lowered tides; providing a much higher value for the bed shear stress. The Generalised Linear Model and Proportional Hazards Model analyses do not indicate any degree of significance ($p > 0.89$) for this bed shear stress variable in relation to the *rate* at which flows recur. However, the significance of bed shear stress in relation to the *specific timing* of individual flows is considerably greater than just considering tidal elevation or river discharge in isolation (Mann–Whitney, $p << 0.0001$; Kolmogorov–Smirnov test, $p << 0.0001$; Table 1). More than 75% of the events seen by the ADCP correspond to the upper 25% of the annual range of the dimensionless bed shear stress variable (Fig. 3). Thus, bed shear stress may govern the instantaneous triggering of an individual flow, but not the rate at which they recur.

5. Discussion

We now discuss the results of the statistical analysis in relation to flow and failure triggering and conditioning. In Table 2 we summarise and compare our findings with the existing hypotheses proposed for slope failure and mass flow triggering at offshore river deltas.

5.1. Extreme river flood discharge leads to delta-lip collapses not hyperpycnal flows

Suspended sediment concentrations are unlikely to be high enough to generate dense, plunging hyperpycnal flow from direct river discharge at the Squamish Prodelta and other rivers in the fjords of British Columbia (Bornhold et al., 1994; Mulder and Syvitski, 1995; Hill et al., 2008). Extreme peaks in river discharge, with suspended sediment concentrations of <1 kg/m^3 (Syvitski et al., 1987), did not trigger hyperpycnal flows, rather they correspond with large ($>20{,}000$ m^3) delta-lip failures a few hours after the flood peak (Fig. 6). If the ADCP data were used in isolation, a hyperpycnal flow may have been interpreted as the initiating process from a broad correspondence in timing. This important observation is only possible due to the repeated MBES surveys which identified the occurrence of delta-lip failures. This type of MBES data is typically not available, and it illustrates a need for caution in assuming that submarine flows that occur during river floods are solely triggered by plunging hyperpycnal flood-water.

During periods of extreme discharge the river delivers sediment to the delta top and lip, but it does not immediately trigger turbidity currents on the offshore delta slope. Instead, sediment rapidly builds up to prograde the delta-lip over a period of hours, prior to a delta-lip collapse.

Hughes Clarke et al. (2014) noted that wholescale plunging of river water was not possible, but did image sediment settling downwards from a surface plume using water column echosounders. It is inferred that convective fingering is responsible for this settling, which can occur at densities of <1 kg/m^3 (Yu et al., 2000; Parsons et al., 2001). Optical backscatter measurements, coupled with conductivity, temperature and density (CTD) profiling, indicate that the upper parts of some turbidity currents are less dense than the surrounding water (Hughes Clarke et al., 2014). This density contrast may be explained by freshwater becoming entrained by sediment that settles out from the river discharge plume. As the mixture crosses the pycnocline, the sediment settles out and may start to flow downslope under its excess density. In the later stages of the flow, as sediment drops out due to deceleration, the entrained freshwater becomes net buoyant as it is less dense than the lowermost sediment-rich layer and also the overlying seawater; it therefore lofts (Sparks et al., 1993). The lower-most (<2 m) part of the flow, which is presumably where the majority of sediment is transported, is not imaged by the optical backscatter measurements (Hughes Clarke et al., 2014). This mechanism of sediment settling may be important for the triggering of flows that are not associated with an obvious failure scarp (Hughes Clarke et al., 2014).

5.2. Conditioning and triggering of delta-lip collapses

The triggering of delta-lip collapses relates to a combination of factors, but a seismic trigger with magnitude $M_L < 3.3$ can be ruled out for the time interval studied (Fig. 3). The cumulative effects of both river discharge and tidal drawdown are shown to precondition and trigger delta-lip failures (Fig. 8). We suggest that two different triggering mechanisms operate, depending on the sediment supply provided by the river. Hence these mechanisms may provide insights into the triggers of slope failures at deltas both with both low and high rates of sediment supply. In the early part of the freshet (prior to mid-June), the background river discharge is low, and hence so is the sediment discharge (Hickin, 1989). Moderate progradation (<5 m) and vertical loading (<2 m) of the delta-lip may initiate preconditioning to failure, but the influence of extreme low spring tides appears to be the dominant control on generating transient excess pore pressures that provide the near-instantaneous trigger (Fig. 8). However, once the river bedload increases in the freshet-peak (mid-June to August), sediment delivery causes major cumulative progradation (up to 30 m) and vertical loading (up to 12 m) at the delta-lip. Pore pressures do not have time to dissipate under such loading, and are raised further following sudden sediment delivery at river flood peaks. Following these peaks, there is a lag of 8–12 h, after which a delayed delta-lip collapses occurs independent of tidal elevation (Fig. 8). Our analysis assumes effective vertical drainage pathways for pore pressure dissipation, and hence homogeneous permeability. However, preconditioning for delayed failures may also be in part due to the presence and geometry of relatively lower permeability layers, below which pore pressures can build up through time (Özener et al., 2009). Such delayed slope failures may be common, particularly at the offshore deltas of high discharge rivers, but have rarely been recognised because of the lack of temporally well-constrained data. However, a series of sequential seafloor cable breaks in the Gaoping submarine canyon offshore Taiwan occurred three days after a major peak in river discharge related to Typhoon Morakot (Carter et al., 2014). The breaks occurred under normal river discharge conditions; hence, it is interpreted that a delayed failure occurred leading to remobilisation of sediment that had rapidly accumulated at the peak in river discharge (Carter et al., 2014).

Table 2
Natural triggering mechanisms hypothesised for slope failures and flows at offshore river deltas.

Control	Trigger mechanism *(cross-referenced to Fig. 1)*	Nature of failures/flows	Reference	Evidence at Squamish prodelta as a trigger?
River discharge	Direct plunging of river water as hyperpycnal flow *(1)*.	Near-continuous flows coincident with peak of flood event.	Mulder and Syvitski (1995); Mulder et al. (2003); Bornhold et al. (1994).	Not a trigger for the largest flows, which are triggered by failures. Sediment concentrations too low in river.
	Localised mixing of the freshwater-saline interface causes enhanced settling of sediment due to convective fingers *(2)*.	Episodic flows coincident with periods of enhanced settling from a surface plume.	Parsons et al. (2001); Hughes Clarke et al. (2014); Hughes Clarke (2016).	Possible trigger, but not for the largest flows, which are triggered by failures.
	Delta failure: Sediments reside temporarily on parts of the delta slope to be later remobilised as they become more unstable *(3)*.	Turbidity currents following main flood event.	Bornhold et al. (1994); Hughes Clarke et al. (2012a, 2014).	Yes.
	Elevated river discharge enhance bed shear stresses, causing erosion and increased flux of bedload driven over the delta lip *(9)*. Can be exaggerated during low tides.	River discharge sweeps accumulated coarse-grained bar and channel sediments (with any bedload) directly onto the steep delta front slopes.	Prior and Bornhold (1989); Bornhold et al. (1994).	Yes.
	Grain avalanches: Bedload swept offshore may avalanche down steeply-inclined foresets on Gilbert-type delta *(10)*.	Sediment accelerates down inclined forsets and transitions into a turbidity current.	Gilbert (1885); Postma et al. (1988).	Possible trigger.
Tides	Excess pore pressures in low permeability materials during low tides triggers liquefaction *(4)*.	Transient pore pressure changes cause liquefaction which leads to slope instability (unlikely to have any effect >1 m below seafloor).	Johns et al. (1986); Chillarige et al. (1997).	No, because failure occurs too deep (>10 m) in sediment.
	Tidal drawdown on gaseous sediments causes expansion and slope failure *(5)*.	Reduction in effective stress during lowered tides where gas can be brought out of solution to trigger deep-seated failure.	Christian et al. (1997); Chillarige et al. (1997); Hughes Clarke et al. (2012a, 2014).	Possible trigger, but not for all failures.
	Lowered tide constricts delta-top channel and enhances bed shear stresses, causing erosion and increased flux of bedload driven over the delta lip *(9)*. Can be exaggerated during high river discharges.	Constriction of channel leads to elevated bed shear stresses causing erosion, and deposition on delta-lip or triggering of sediment avalanches.	Prior and Bornhold (1989); Hughes Clarke et al. (2012a, 2014); Hughes Clarke (2016).	Possible trigger for flows as sediment is flushed offshore.
Storm waves	Cyclic loading of delta-lip sediments induces slope failure *(7)*.	Transient pore pressure changes cause liquefaction.	Prior et al. (1989).	No.
Upper to mid-prodelta processes	Localised liquefaction or breaching within submarine channels or incision of steep margins by previous flow *(8)*.	Triggers turbidity current on prodelta slope.	Van Den Berg et al. (2002); Mastbergen and Van Den Berg (2003).	Possible trigger for many major and minor bedform events that do not have obvious failure scarps.
Earthquakes	Strong ground motion and development of transient excess pore pressures *(6)*.	Destabilisation of slope sediments due to shaking, liquefaction or strain softening.	Prior and Bornhold (1989); Bornhold and Prior (1989); Bornhold et al. (1994).	Not a trigger during 2011 surveyed period.

The spatial distribution of the five delta-lip collapses also appears to be important in determining the temporal sequence of their occurrence (Fig. 4). Delta-lip collapse A occurred near the most seaward extent of the delta lip following progradation due to sediment build up. Removal of failed sediment oversteepened its western flank, where delta-lip collapse B occurred 14 days later. Sediment continued to build up on the delta-lip, until the post-failure morphology was no longer visible. The extent of the next collapse, C at JD181 corresponded to the first major peak in river discharge. It covered areas that failed during lip-collapses A and B. This may indicate that loose sediment, rapidly-deposited over the previous failure scars, was more susceptible to failure. Eight days later, delta-lip collapse D occurred at the seaward extent of the delta-lip which adjoined the eastern flank of collapse C's head-scarp. The final collapse, E, occurred 46 days later, also at the most seaward extent of the delta-lip. It covering a similar area to collapse C; which was also an area of loose, recently deposited sediments that may have been more prone to fail.

5.3. River discharge is the primary conditioner for turbidity current activity

River discharge is identified as a strongly significant individual variable in relation to both turbidity current timing and recurrence rate. The Proportional Hazards Model for the ADCP-observed flows indicate the rate at which turbidity currents occur increases by 0.6% (+/−0.4%; 95% confidence intervals) for every 1 m^3/s increase in river discharge. This only holds for conditions where the river discharge exceeds a minimum threshold – defined here as the mean annual river discharge (~253 m^3/s).

5.4. Tidal effects amplify the effects of river discharge to trigger turbidity currents

Lowered tides are shown to have a significant relationship with turbidity current timing, albeit less significant than river discharge. This is presumably because sediment supply from the river is the

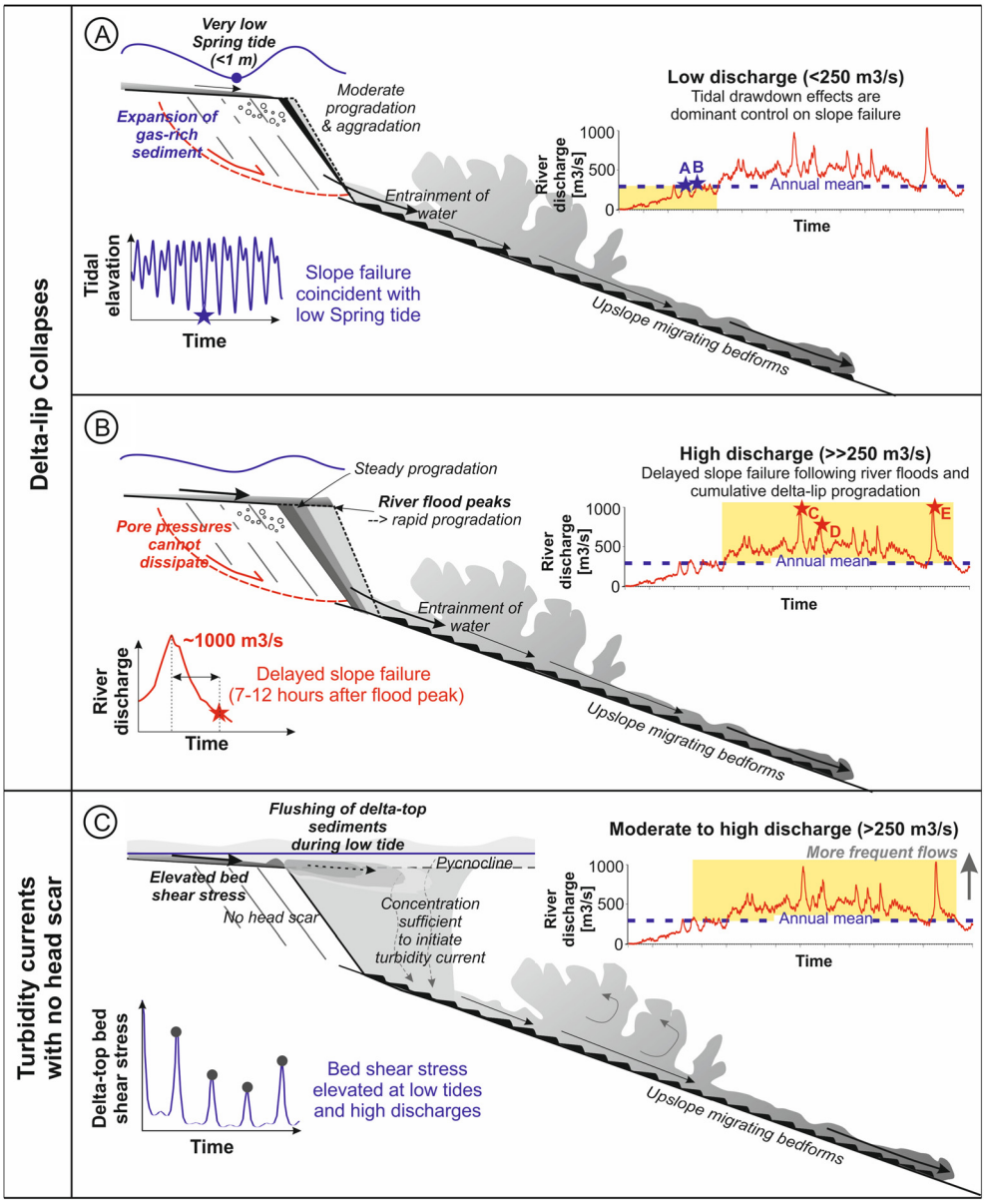

Fig. 8. Illustration of mechanisms inferred to be responsible for triggering of delta-lip collapses. (A and B) Events associated with headscars, triggered during low rates of delta-lip progradation (A) and high rates of progradation (B). (C) Events which are not associated with headscars and thus slope failure, nor with hyperpycnal river discharge.

main control on turbidity current frequency. We suggest that tidal effects may enhance the effects of river discharge in two ways. In the first, additive or sequential effects are significant, such that the slope is preconditioned by increased sediment load and tidal influence (e.g. pore pressure change). This addition of two effects then tips the balance to trigger a failure. The second scenario is related to amplified effects, where combinations of low tides and elevated river discharge enhance bed shear stresses, causing erosion and increased flux of bedload driven over the delta lip. Given the low river discharge early in the season, the contribution of lower tides is likely to be the more important factor. Only a relatively small amount of shear stress is necessary at the start of the freshet to flush the mouth bar accumulated over the winter. The significance of tidal effects will reduce as river discharge increases throughout the freshet, amplifying bed shear stresses and increasing the likelihood of seaward flushing of delta-top sediments. This flushing, coupled with the near-constant settling of convective fingers of sediment, then triggers flows on the upper prodelta slope. This mechanism is thus distinct from a hyperpycnal flow trigger and does not require a slope failure that forms a headscarp. This mechanism may explain why a damaging turbidity current occurred on the Fraser River delta-slope, yet no headscarp was identified (Lintern et al., 2016). The flow was capable of displacing a one tonne seafloor observatory and severed an armoured cable.

6. Conclusions

Here we analyse the first field data that provides the timings of >100 failure and turbidity currents, from Squamish Prodelta. The largest peaks in river discharge did not result in hyperpycnal flows, rather they caused more rapid progradation of the delta front, which ultimately led to large delayed delta-lip collapses (>20,000 m^3/s). Sedimentation on the delta-top and progradation of the delta-lip appear to precondition the slope to failure. The ultimate trigger is then either due to exacerbation of pore pressures on the slope via tidal drawdown effects, or rapid sedimentation during river floods. As suggested qualitatively by Hughes Clarke et al. (2012a, 2012b), elevated river discharge is now quantitatively

demonstrated to be a primary control for the 'switch on' of turbidity current activity. River discharge is a statistically significant variable in explaining the frequency at which turbidity currents occur. Each 1 m^3/s increase in discharge above the threshold discharge (mean annual level) corresponds to a 0.6% increase in flow likelihood. Below that level the system is 'switched off'. Tidal elevation also contributed to the timing of turbidity currents. This is most likely due to amplification of the effect of river discharge causing elevated bed shear stresses on the delta-lip, and seaward flushing of delta-top sediments.

Acknowledgements

We thank David Piper, Thomas Hubble, one anonymous reviewer and Editor Martin Frank for their insightful reviews, which substantially improved the manuscript. We acknowledge the following grants: NERC International Opportunities Fund (NE/M017540/1) "Coordinating and pump-priming international efforts for direct monitoring of active turbidity currents at global test sites"; and NERC Environmental Risks to Infrastructure Innovation Programme (ERIIP) (NE/N012798/1) "What threat do turbidity currents and submarine landslides pose to strategic submarine telecommunications cable infrastructure". Talling was supported by a NERC and Royal Society Industry Fellowship hosted by the International Cable Protection Committee (ICPC).

Appendix. Supplementary material

Appendix A (expanded methods) and Appendix B (full statistics results) can be found online at http://dx.doi.org/10.1016/j.epsl.2016.06.021. Animated timelapse bathymetry for the multibeam surveys on the upper part of the prodelta can be found online at http://www.omg.unb.ca/Projects/SQ_2011_html/.

References

Bhattacharya, J.P., Giosan, L., 2003. Wave-influenced deltas: geomorphological implications for facies reconstruction. Sedimentology 50 (1), 187–210.

Bornhold, B.D., Prior, D.B., 1989. Sediment blocks on the sea floor in British Columbia fjords. Geo Mar. Lett. 9 (3), 135–144.

Bornhold, B.D., Ren, P., Prior, D.B., 1994. High-frequency turbidity currents in British Columbia fjords. Geo Mar. Lett. 14 (4), 238–243.

Bromhead, E., 2006. The Stability of Slopes. CRC Press.

Carter, L., Gavey, R., Talling, P., Liu, J., 2014. Insights into submarine geohazards from breaks in subsea telecommunication cables. Oceanography 27, 58–67. http://dx.doi.org/10.5670/oceanog.2014.40.

Chillarige, A.V., Morgenstern, N.R., Robertson, P.K., Christian, H.A., 1997. Seabed instability due to flow liquefaction in the Fraser River delta. Can. Geotech. J. 34, 520–533. http://dx.doi.org/10.1139/T97-019.

Christian, H.A., Mosher, D.C., Mulder, T., Barrie, J.V., Courtney, R.C., 1997. Geomorphology and potential slope instability on the Fraser River delta foreslope, Vancouver, British Columbia. Can. Geotech. J. 34 (3), 432–446.

Clare, M.A., Talling, P.J., Challenor, P., Malgesini, G., Hunt, J., 2014. Distal turbidites reveal a common distribution for large (>0.1 km^3) submarine landslide recurrence. Geology, G35160-1.

Clare, M.A., Talling, P.J., Challenor, P.G., Hunt, J.E., 2016. Tempo and triggering of large submarine landslides: statistical analysis for hazard assessment. In: Submarine Mass Movements and Their Consequences. Springer International Publishing, pp. 509–517.

Cooper, C., Wood, J., Andrieux, O., 2013. Turbidity current measurements in the Congo Canyon. In: Proceedings of Offshore Technology Conference. 1–4 May 2013, Houston, Texas.

Dietrich, P., Ghienne, J.F., Normandeau, A., Lajeunesse, P., 2016. Up-slope migrating bedforms in a proglacial sandur delta: cyclic steps from river-derived underflows? J. Sediment. Res. 86, 113. http://dx.doi.org/10.2110/jsr.2016.4.

Droxler, A.W., Schlager, W., 1985. Glacial versus interglacial sedimentation rates and turbidite frequency in the Bahamas. Geology 13 (11), 799–802.

Forel, F.A., 1888. Le ravin sous-lacustre du Rhône dans le lac Léman. Bull. Soc. Vaud. Sci. Nat. 23, 85–107.

Gilbert, G.K., 1885. The topographic features of lake shores U.S. In: United States Geological Survey Annual Report, vol. 5, pp. 75–123.

Hickin, E.J., 1989. Contemporary Squamish River sediment flux to Howe Sound, British Columbia. Can. J. Earth Sci. 26 (10), 1953–1963.

Hill, P.R., Conway, K., Lintern, D.G., Meulé, S., Picard, K., Barrie, J.V., 2008. Sedimentary processes and sediment dispersal in the southern Strait of Georgia, BC, Canada. Mar. Environ. Res. 66, S39–S48.

Hughes Clarke, J.E., 2016. First wide-angle view of channelized turbidity currents linking migrating cyclic steps to flow characteristics. Nat. Commun. 7, 118960. http://dx.doi.org/10.1038/ncomms11896.

Hughes Clarke, J.E., Brucker, S., Muggah, J., Church, I., Cartwright, D., Kuus, P., Eisan, B., 2012a. The Squamish Prodelta, monitoring active landslides and turbidity currents. In: Canadian Hydrographic Conference.

Hughes Clarke, J., Brucker, S., Muggah, J., Hamilton, T., Cartwright, D., Church, I., Kuus, P., 2012b. Temporal progression and spatial extent of mass wasting events on the Squamish prodelta slope. In: Eberhardt, et al. (Eds.), Landslides and Engineered Slopes: Protecting Society through Improved Understanding. Taylor & Francis Group, London, ISBN 978-0-415-62123-6, pp. 1091–1096.

Hughes Clarke, J.E., Marques, C.R.V., Pratomo, D., 2014. Imaging active mass-wasting and sediment flows on a fjord delta, Squamish, British Columbia. In: Submarine Mass Movements and Their Consequences, vol. 37. Springer International Publishing, pp. 249–260.

Ingersoll, R.V., Dickinson, W.R., Graham, S.A., 2003. Remnant-ocean submarine fans: largest sedimentary systems on Earth. In: Special Papers – Geological Society of America, vol. 370, pp. 191–208.

Johns, M.W., Prior, D.B., Bornhold, B.D., Coleman, J.M., Bryant, W.R., 1986. Geotechnical aspects of a submarine slope failure, Kitimat Fjord, British Columbia. Mar. Georesour. Geotechnol. 6 (3), 243–279.

Kramer, S.L., 1988. Triggering liquefaction flow slides in coastal soil deposits. Eng. Geol. 26, 17–31.

Lambe, T.W., Whitman, R.V., 2008. Soil Mechanics SI Version. John Wiley & Sons.

Lambert, A., Giovanoli, F., 1988. Records of riverbome turbidity currents and indications of slope failures in the Rhone delta of Lake Geneva. Limnol. Oceanogr. 33 (3), 458–468.

Lintern, D.G., Hill, P.R., Stacey, C., 2016. Powerful unconfined turbidity current captured by cabled observatory on the Fraser River delta slope, British Columbia, Canada. Sedimentology. http://dx.doi.org/10.1111/sed.12262.

Mastbergen, D.R., Van Den Berg, J.H., 2003. Breaching in fine sands and the generation of sustained turbidity currents in submarine canyons. Sedimentology 50, 625–637. http://dx.doi.org/10.1046/j.1365-3091.2003.00554.x.

Mulder, T., Syvitski, J.P., 1995. Turbidity currents generated at river mouths during exceptional discharges to the world oceans. J. Geol. 103, 285–299.

Mulder, T., Syvitski, J.P., Migeon, S., Faugeres, J.C., Savoye, B., 2003. Marine hyperpycnal flows: initiation, behavior and related deposits. A review. Mar. Pet. Geol. 20, 861–882. http://dx.doi.org/10.1016/j.marpetgeo.2003.01.003.

Orton, G.J., Reading, H.G., 1993. Variability of deltaic processes in terms of sediment supply, with particular emphasis on grain size. Sedimentology 40 (3), 475–512.

Özener, P.T., Özaydın, K., Berilgen, M.M., 2009. Investigation of liquefaction and pore water pressure development in layered sands. Bull. Earthq. Eng. 7 (1), 199–219.

Parsons, J.D., Bush, J.W., Syvitski, J.P., 2001. Hyperpycnal plume formation from riverine outflows with small sediment concentrations. Sedimentology 48 (2), 465–478.

Piper, D.J., Normark, W.R., 2009. Processes that initiate turbidity currents and their influence on turbidites: a marine geology perspective. J. Sediment. Res. 79 (6), 347–362.

Postma, G., Nemec, W., Kleinspehn, K.L., 1988. Large floating clasts in turbidites: a mechanism for their emplacement. Sediment. Geol. 58 (1), 47–61.

Pratomo, D.G., 2016. Coupling of repetitive multibeam surveys and hydrodynamic modelling to understand bedform migration and delta evolution. PhD thesis. University of New Brunswick.

Prior, D.B., Bornhold, B.D., 1989. Submarine sedimentation on a developing Holocene fan delta. Sedimentology 36 (6), 1053–1076.

Prior, D.B., Bornhold, B.D., Wiseman, W.J., Lowe, D.R., 1987. Turbidity current activity in a British Columbia fjord. Science 237 (4820), 1330–1333.

Prior, D.B., Coleman, J.M., Bornhold, B.D., 1982. Results of a known seafloor instability event. Geo Mar. Lett. 2 (3–4), 117–122.

Prior, D.B., Suhayda, J.N., Lu, N.Z., Bornhold, B.D., Keller, G.H., Wiseman, W.J., Wright, L.D., Yang, Z.S., 1989. Storm wave reactivation of a submarine landslide. Nature 341 (6237), 47–50.

Sparks, R.S.J., Bonnecaze, R.T., Huppert, H.E., Lister, J.R., Hallworth, M.A., Mader, H., Phillips, J., 1993. Sediment-laden gravity currents with reversing buoyancy. Earth Planet. Sci. Lett. 114 (2), 243–257.

Stronach, J., Zaremba, L., Wong, M., Neil, L., McLennan, N., 2006. Wave and current forecast system for the mouth of the Fraser River. Hay and Company Consultants, Vancouver. 15 pp.

Symons, W.O., Sumner, E.J., Talling, P.J., Cartigny, M.J., Clare, M.A., 2016. Large-scale sediment waves and scours on the modern seafloor and their implications for the prevalence of supercritical flows. Mar. Geol. 371, 130–148.

Syvitski, J.P., Burrell, D.C., Skei, J.M., 1987. Fjords: Processes and Products. Springer Science & Business Media.

Syvitski, J.P., Shaw, J., 1995. Sedimentology and geomorphology of fjords. Dev. Sedimentol. 53, 113–178.

Talling, P.J., Allin, J., Armitage, D.A., Arnott, R.W., Cartigny, M.J., Clare, M.A., et al., 2015. Key future directions for research on turbidity currents and their deposits. J. Sediment. Res. 85 (2), 153–169.

Terzaghi, K., 1943. Theoretical Soil Mechanics. John Wiley and Sons, New York. 510 pp.

Van Den Berg, J.H., Van Gelder, A., Mastbergen, D.R., 2002. The importance of breaching as a mechanism of subaqueous slope failure in fine sand. Sedimentology 49 (1), 81–95.

Wright, L.D., 1977. Sediment transport and deposition at river mouths: a synthesis. Geol. Soc. Am. Bull. 88 (6), 857–868.

Xu, J.P., Noble, M.A., Rosenfeld, L.K., 2004. In-situ measurements of velocity structure within turbidity currents. Geophys. Res. Lett. 31 (9).

Xu, J.P., Sequeiros, O.E., Noble, M.A., 2014. Sediment concentrations, flow conditions, and downstream evolution of two turbidity currents, Monterey Canyon, USA. Deep-Sea Res., Part 1, Oceanogr. Res. Pap. 89, 11–34.

Yu, W.S., Lee, H.Y., Hsu, S.M., 2000. Experiments on deposition behavior of fine sediment in a reservoir. J. Hydraul. Eng. 126 (12), 912–920.